Machine Learning Based Estimation of Complex Permittivity of Planetary Rock and Regolith Materials

Dante Miller[1] Rice University
Deshpande Manohar[2] NASA

Abstract

Synthetic Aperture Radar (SAR) plays a crucial role in advancing our understanding of ice formations, natural resources, and planetary processes. Nevertheless, a critical challenge in utilizing SAR technology lies in comprehending how materials and objects respond to applied electromagnetic waves. By gaining insights into the responses of various materials and objects to electromagnetic waves at different frequencies and orientations, information retrieval algorithms, such as those employed in SAR systems, can be designed to effectively capture the required signals from materials or objects of interest. Optimizing existing numerical methods for characterizing these responses is essential. In this study, we apply and compare a Feedforward Neural Network (FNN) and XGBoost models to simulated data to make precise predictions, with the aim of enhancing efficiency and accuracy in the design of SAR algorithms using both simulated and actual data.

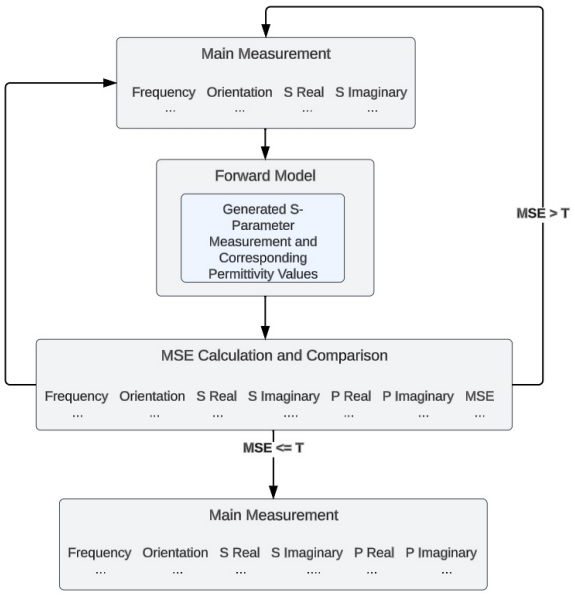

Figure 1. Illustration of the Brute Force Approach for Estimating Permittivity

1. Introduction

1.1. Background

s Synthetic Aperture Radar (SAR) is a radar imaging technology that transmits electromagnetic waves toward a target, captures and interprets the reflected radar signals using an antenna mounted on a moving platform (Moreira et al., 2013). Understanding ice formations, natural resources and dynamic processes on Earth and other planetary bodies has been made possible through SAR systems (Sun et al., 2022).

The demand for developing new retrieval algorithms, particularly automated ones, is becoming more challenging. Nevertheless, as remote sensing data becomes more readily accessible and retrieval techniques advance, there is an anticipation that the automation and reliability of SAR data analysis will see significant improvements in the near future (Shen et al., 2019). To enhance these algorithms significantly, it is essential to develop a more profound understanding of how materials or areas respond to their interaction with applied electromagnetic waves. This understanding plays a pivotal role in the development of effective retrieval algorithms.

Materials respond to an applied radar signal in two ways, a real and imaginary component known as the complex dielectric property (Bonello et al., 2020). The real component signifies the material's capacity to store energy, while the imaginary component denotes its ability to absorb and convert energy into heat. To determine the real and imaginary permittivity for a given material, we have to reconstruct it using a set of coefficients known as s-parameters that describe the reflection and transmission of an applied radar signal by placing a material in a sample holder of a coaxial transmission line or in a coaxial-circular wave guide (Gorriti & Slob, 2005). The real and imaginary permittivity can be computed using an optimization procedure that consists of minimizing a cost function involving the measured s-parameters and a mathematical model that estimates the s-parameters and

permittivity of the material.

The optimization method we consider is similar to the procedure described in (Gorriti & Slob, 2005). In our case, the s-parameter measurement dataset exhibiting the lowest Mean Squared Error (MSE) in comparison to the measured s-parameter data will be used in conjunction with the permittivity estimation process for both real and imaginary parts. This process can be noticed in Figure 1.

To optimize this process, we are exploring two distinct approaches: one based on a neural network and another based on XGBoost. In (Bonello et al., 2020) and (Mosavirik et al., 2022), they utilized a Feedforward Neural Network (FNN) to predict the complex permittivity of biological tissues and materials.

We aim to investigate whether we can model the complex dielectric properties of a materials or areas using an FNN. However, as FNNs are primarily designed for creating new representations of non-tabular data, and our data is in tabular format, we are also considering XGBoost, which is specifically designed to handle this type of data (Shwartz-Ziv & Armon, 2022). It's worth noting that traditionally, obtaining a comprehensive characterization of a planetary sample typically necessitates between 25 to 50 distinct orientation measurements [CITATION NEEDED]. Our two distinct approaches: one based on a neural network and another based on XGBoost are designed to substantially enhance the efficiency and accuracy of complex permittivity estimation.

Within the scope of this paper, we investigate specialized materials, namely Moon rock sample 14304 and the Martian meteorite SAU008. These materials provide unique insights into the geological compositions of celestial bodies beyond Earth. The understanding and optimization of complex permittivity in SAR analysis have the potential to greatly enhance our ability to explore and comprehend the dynamic processes taking place on Earth and other planetary surfaces.

2. Method

2.1. Measurement and Data Collection

Start by explaining how the measurement data is collected. Detail the experimental setup, equipment used, and measurement procedures. Mention the specific tools or instruments employed to capture SAR data or other relevant radar signals. [CITATION NEEDED]

2.2. Specialized Materials

2.2.1. Moon Rock - 14304

Moon rock - 14304, a sample collected during the Apollo mission, has led to speculation regarding the possible presence of granite on the Moon. This, in turn, hints at a lunar geological history that could involve processes like magma intrusion, gradual cooling, and mineral crystallization [CITATION NEEDED].

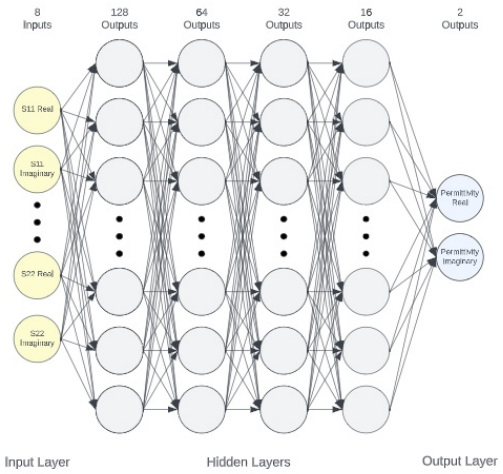

Figure 2. Illustration of the Neural Network Approach for Estimating Permittivity

2.2.2. Martian Meteorite - SAU008

Martian meteorite - SAU008, a meteorite sample originating from the planet Mars, provides valuable insights into the geological and geochemical characteristics of Mars [CITATION NEEDED].

2.3. Feedforward Neural Network and XGBoost Model Implementation

2.3.1. Experiment Task

The primary objective of this study was to develop FNN and XGBoost models capable of estimating the complex permittivity of planetary materials based on their s-parameter measurements. This task involved training the models to learn the underlying relationships between s-parameter measurements and complex permittivity values.

2.3.2. Data

In this study, two types of data were employed: simulated and actual samples from Moon rock - 14304 and Martian meteorite - SAU008. Each observation in the dataset represents a measurement for the material sample at a specific orientation and frequency.

The number of observations in both the simulated and actual datasets are provided in Table 1. To facilitate model evaluation, we applied a train-val-test split to segregate the

Dataset	Data Type	Number of Observations
Moon	Simulated Training	320320
	Simulated Validation	64064
	Simulated Testing	16016
	Actual Test	4004
Meteorite	Simulated Training	1601600
	Simulated Validation	320320
	Simulated Testing	81081
	Actual Test	4004

Table 1. Number of Observations in Moon and Meteorite Datasets

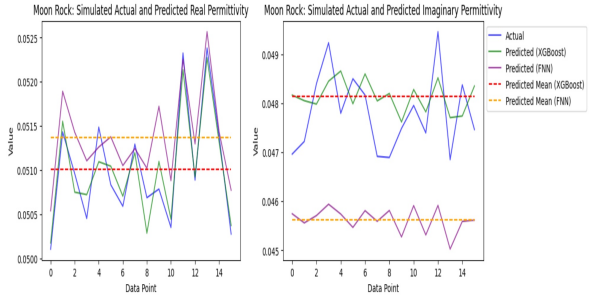

Figure 3. Moon Simulated Model Prediction Summary

simulated data into sets designated for assessing the model's performance on simulated data. Refer to Table 1 for further details.

2.3.3. Preprocessing

In terms of preprocessing, we began by normalizing the real permittivity values. Additionally, we applied quantile transformation to the scatter parameters within the training dataset, ensuring that the testing dataset was transformed to align with its distribution. Furthermore, it's worth noting that the train-val-test splits were conducted by selecting random observations from the entirety of measurements."

2.3.4. Implementation

The overall implementation can be observed in Figure 2. This neural network architecture consists of eight inputs representing the s-parameters. These inputs are mapped to nodes in the subsequent layer, which includes four hidden layers. The output of the final hidden layer is mapped to real and imaginary permittivity values. Essentially, the model learns to map each independent observation to corresponding real and imaginary permittivity values. Additionally, a baseline XGBoost model was employed, utilizing the default settings from the XGBoost module, with the only modification being an increase in the number of estimators to 250.

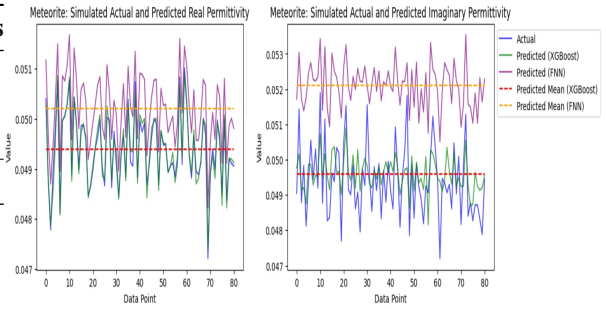

Figure 4. Meteorite Simulated Model Prediction Summary

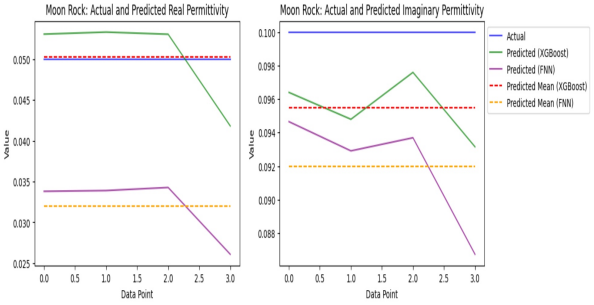

Figure 5. Moon Rock Actual Model Prediction Summary

3. Software and Data Availability

The data and code for predicting permittivity (real and imaginary) are available in the GitHub repository at:

https://github.com/DanteMillerDS/NASA-Material-Classifier

4. Results

In Figure 3, we conducted training of the FNN and XGBoost models using the train-validation-test splits presented in Table 1. During the evaluation phase, as depicted in Figure 3, we observed that for simulated moon samples, the XGBoost model's predicted values closely approximate the actual values. Conversely, the FNN exhibits slight deviations in this region but does not precisely match the actual values. Similar trends are noticed when examining the predictions for imaginary permittivity values. Moving on to the simulated meteorite samples in Figure 4, we can largely observe the same phenomenon as in Figure 3. These results collectively demonstrate our ability to approximate the simulation s-parameters to their permittivity values reasonably well.

Now, we aim to assess how these models perform in predicting the permittivity of actual s-parameter measurements. As per the data in Table 1, we only possess four sets of measurements for each material. Our objective is to characterize a material using these limited four orientations, although it was previously mentioned that around 25-50

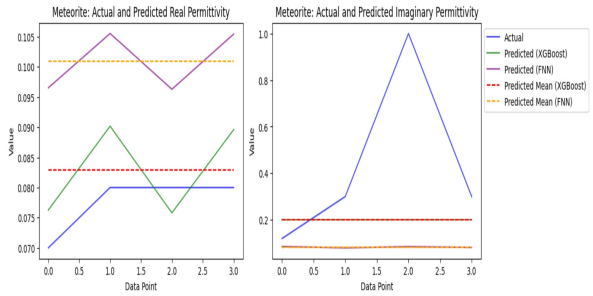

Figure 6. Meteorite Actual Model Prediction Summary

unique orientations are needed for comprehensive material characterization.

In Figure 5, we apply both the FNN and XGBoost models to actual moon rock data. Notably, the predicted values closely align with the actual values, suggesting our ability to accurately identify the permittivity value for moon rock based on simulated data. Turning to Figure 6, when examining the predicted results for the real permittivity of the meteorite, it becomes evident that the XGBoost predictions are close to the actual permittivity values. The FNN, while slightly further off, still exhibits a reasonable degree of proximity. However, when looking at the predictions for imaginary permittivity values, it appears that multiple potential values exist. The FNN approximates the permittivity value associated with the first orientation relatively well, whereas XGBoost maintains a constant value across all orientations. This phenomenon concerning imaginary permittivity distribution is not present in the simulation data, which is limited to the range of 0 to 1. Consequently, it does not account for permittivity values exceeding 0.1 but does establish that the permittivity surpasses the maximum value, a characteristic captured by both the FNN and XGBoost models.

5. Conclusion

Based on our findings, several key points emerge:

1. We can efficiently model the relationship between s parameters and permittivity, both real and imaginary, by leveraging both simulated and actual data. This approach enables us to identify these permittivity values with significantly reduced computational time compared to traditional methods.

2. Our methodology allows for the estimation of real and imaginary permittivity values in newly measured data, leveraging the insights gained from our analysis of simulated data. This approach offers a cost-effective solution for characterizing materials in real-world scenarios.

3. Importantly, our results demonstrate that neural networks can yield accuracy comparable to that of existing brute-force methods, making it a viable and efficient alternative for estimating complex permittivity values.

6. Future Direction

In (Komarov et al., 2005), it is highlighted that complex dielectric properties are subject to various influencing factors, including frequency, temperature, and moisture content. This implies that when we receive scattering parameters at a specific orientation and frequency, they correspond to particular permittivity values in both the real and imaginary components. This results in a continuous range of values associated with a set of S-parameter measurements.

In our specific case, we have maintained constant permittivity values, but we propose that allowing them to vary continuously could lead to an enhanced overall measurement of the real and imaginary permittivity values. This notion is supported by (Komarov et al., 2005), which underscores that dielectric properties exhibit significant variation with frequency. The frequency-dependent trends in dielectric properties can furnish critical insights into material characteristics.

In our current analysis, which encompasses both simulated and actual data, we did not account for the frequency-dependent permittivity values. However, we believe that modeling frequency-specific relationships while considering distinct permittivity values could potentially bolster the performance of our overall model. Figure 1 illustrates this point, showing an absence of correlation between the S-parameters and permittivity. Yet, when we delve into frequency-specific relationships, a more discernible pattern emerges. This observation leads us to suggest that permittivity values exhibit frequency-specific behavior, and by accommodating fluctuating real and imaginary permittivity, we may anticipate improved results. Additionally, we did not consider orientation and frequency as inputs to the models, only modeling the S-parameters, as depicted in Figure 2.

References

Bonello, J., Demarco, A., Farhat, I., Farrugia, L., and Sammut, C. V. Application of artificial neural networks for accurate determination of the complex permittivity of biological tissue. *Sensors (Basel, Switzerland)*, 20(16):4640, 2020. doi: 10.3390/s20164640. URL https://www.ncbi.nlm.nih.gov/pmc/articles/PMC7472264/.

Gorriti, A. and Slob, E. Comparison of the different reconstruction techniques of permittivity from s-parameters. *IEEE Transactions on Geoscience and Remote Sensing*, 43(9):2051–2057, 2005. doi: 10.1109/TGRS.

2005.854312. URL "https://ieeexplore.ieee.org/document/1499021".

Komarov, V., Wang, S., and Tang, J. Permittivity and measurement. *Encyclopedia of RF and Microwave Engineering*, pp. 3693–3711, 01 2005. URL https://www.researchgate.net/publication/281304882_Permittivity_and_measurementf.

Moreira, A., Prats-Iraola, P., Younis, M., Krieger, G., Hajnsek, I., and Papathanassiou, K. P. A tutorial on synthetic aperture radar. *IEEE Geoscience and Remote Sensing Magazine*, 1(1):6–43, 2013. doi: 10.1109/MGRS.2013.2248301. URL https://ieeexplore.ieee.org/stamp/stamp.jsp?tp=&arnumber=6504845.

Mosavirik, T., Hashemi, M., Soleimani, M., Nayyeri, V., and Ramahi, O. M. Material characterization using power measurements: Miracle of machine learning. pp. 606–609, 2022. doi: 10.23919/EuMC50147.2022.9784321. URL https://ieeexplore.ieee.org/abstract/document/9784321?casa_token=8yPFlnZImJ0AAAAA:-esmatdgAi6AVQM0HZt9WlBJosk4grDwbJxrp87I0D6Ha9LO7BFLPqWobatKzQX4FfDFoEaX.

Shen, X., Wang, D., Mao, K., Anagnostou, E., and Hong, Y. Inundation extent mapping by synthetic aperture radar: A review. *Remote Sensing*, 11(7), 2019. ISSN 2072-4292. doi: 10.3390/rs11070879. URL https://www.mdpi.com/2072-4292/11/7/879.

Shwartz-Ziv, R. and Armon, A. Tabular data: Deep learning is not all you need. *Information Fusion*, 81:84–90, 2022. URL https://www.sciencedirect.com/science/article/abs/pii/S1566253521002360.

Sun, G.-C., Liu, Y., Xiang, J., Liu, W., Xing, M., and Chen, J. Spaceborne synthetic aperture radar imaging algorithms: An overview. *IEEE Geoscience and Remote Sensing Magazine*, 10(1):161–184, 2022. doi: 10.1109/MGRS.2021.3097894. URL https://ieeexplore.ieee.org/abstract/document/9509575?casa_token=-6BJ0bPU7LQAAAAA:316qF3I_-FyAQDkdH4S5TgXNC43cccVjkRFgv8B813nr4ZtI56wzYrH-Ks3X47lC1k0pC7KE.